DOI:
10.1038/s41377-018-0025-x

Document Version
Peer reviewed version

Generalization of optical theorem: experimental proof for radially polarized beams

Running title: Optical theorem generalization: experimental proof

Authors: Alexey V. Krasavin,[1,*] Paulina Segovia,[1] Rostyslav Dubrovka,[2] Nicolas Olivier,[1] Gregory A. Wurtz,[1] Pavel Ginzburg,[3,4] Anatoly V. Zayats[1]

[1] Department of Physics, King's College London, Strand, London WC2R 2LS, United Kingdom

[2] Department of Electronic Engineering, Queen Mary University of London, United Kingdom

[3] School of Electrical Engineering, Tel Aviv University, Ramat Aviv, Tel Aviv 69978, Israel

[4] ITMO University, St. Petersburg 197101, Russia

Email addresses:

A.V.K.: alexey.krasavin@kcl.ac.uk

P.S.: paulina.segovia_olvera@kcl.ac.uk

R.D.: r.dubrovka@qmul.ac.uk

N.O.: nicolas.olivier@kcl.ac.uk

G.A.W.: g.wurtz@kcl.ac.uk

P.G.: pginzburg@post.tau.ac.il

A.V.Z.: a.zayats@kcl.ac.uk

***Corresponding author contact information:**

Email: alexey.krasavin@kcl.ac.uk

Tel.: +44 (0)20 7848 7065

Fax: +44 (0)20 7848 2420

ABSTRACT: The optical theorem, being a consequence of the energy conservation in scattering processes, directly relates the forward scattering amplitude to the extinction cross-section of the object. Originally derived for planar scalar waves, it neglects the complex structure of the focused beams and vectorial nature of electromagnetic field. On the other hand, radially or azimuthally polarized and various vortex beams essential in modern photonic technologies possess a prominent vectorial field structure. Here we experimentally demonstrate complete violation of the commonly-used form of the optical theorem for radially polarized beams at both visible and microwave frequencies. We show that a plasmonic particle illuminated by such a beam exhibit strong extinction, while the scattering in the forward direction is zero. The generalized formulation of the optical theorem provides agreement with the observed results. The reported effect is important for understanding and designing interaction of complex vector beams carrying longitudinal field components with subwavelength objects important in imaging, communications, nanoparticle manipulation, and detection and metrology.

KEYWORDS: optical theorem; generalization; radial polarization; vectorial beams

INTRODUCTION

The optical theorem is a fundamental relation, emerging in wave scattering phenomena, either classical or quantum [1]. It relates an amplitude of a wave scattered from an object in the forward direction to its extinction cross-section. A rigorous proof of the theorem in the commonly-used form, however, strongly relies on a scalar nature of the considered waves [1] and can be extended to a simple vectorial case of transverse plane waves [2,3,4]. While the former is usually true for acoustic or electron scattering (and even in this cases only for plane waves, as seen in [5]), in the case of electromagnetic waves, both the spatial distribution of the incident field and

its polarization structure can be important. It has been shown that tightly focused Gaussian beams, scattered by a small spherical particle, partially violate the optical theorem [6,7]. This violation is a direct consequence of the appearance of the longitudinal field components at the focal spot where a scattering object is located. The interaction of other beams of vectorial nature, such as radially or azimuthally polarized beams or complex vortex beams carrying optical angular momentum, with various nanostructures was studied both theoretically and experimentally [8,9,10,11], but the dynamics of the scattering of such beams and its relation to the fundamental properties of the optical theorem have not been considered. At the same time, the electromagnetic beams with a complex vectorial nature of the field are used now in numerous important applications including high resolution imaging, radar detection, communication technology, nanoparticle trapping and manipulation, surface metrology and many others for which the optical theorem is widely used in system design and performance evaluation.

Many versions of optical theorem have been formulated for scenarios, involving different geometries of illumination for which a textbook form of the theorem cannot be applied. For example, application of the optical theorem to the scattering in transmission lines has been studied [12] as well as the generalizations for (i) nonlinear, time-varying and lossy materials [13], (ii) anisotropic embedding media [14], (iii) general inhomogeneous media [15], (iv) surface waves and layered media [16], as well (v) including evanescent fields [17] have been theoretically derived. At the same time, in majority of experimental studies, where partial information on scattering can be acquired, the optical theorem still tends to be applied in its conventional form. The goal of this work is to demonstrate experimentally that complete violation of this conventional formulation takes place for vectorial beams and provide an experimental proof of the appropriate generalized version.

Here, exploiting vectorial structure of radially polarized beams, we demonstrate a complete violation of the commonly-used formulation of the optical theorem in both optical and microwave spectral ranges. Studying angular spectra of scattering from subwavelength nanoparticles, we show that scattering in the forward direction, favorable for the linearly polarized light illumination, vanishes under the radially polarized excitation, despite the particle has a significant non-zero extinction cross-section. This makes the prediction of the conventional form of the optical theorem establishing a direct relation between these two quantities inappropriate. The violation of such connection was further confirmed in the experiments for microwave radiation scattering by mapping the amplitude and phase of the forward scattering with a sub-diffraction resolution. The same as in the optical regime, the experimental results, confirmed by numerical simulations, reveal strong overall scattering of the radially polarized beam with no forward scattering detected, in violation of the textbook optical theorem. Finally, the experimental and numerical results verify predictions based on the recent generalizations of the optical theorem formulation.

MATERIALS AND METHODS

Finite element numerical modeling

Numerical analysis was performed using a finite element software (COMSOL Multiphysics). The scattering from a 100 nm spherical gold nanoparticle (a permittivity taken from [18]) was studied in the scattering-field formulation, with the simulation domain surrounded by a perfectly matched layer, to guarantee the absence of back-reflection from the outer domain boundaries. The symmetry of the simulation setup (both the incident field and the object) was used to decrease the computational complexity. The simulation domain, initially having a spherical form was cut by two perpendicular planes intersecting along the beam axis. In the case of the plane

wave illumination, these were the plane of the linear polarization and the plane perpendicular to it. In the case of the radial polarization, the azimuthal orientation of the planes is invariant due to the symmetry of the beam/object system. Only one quadrant of the space between these planes was used for numerical evaluation with the appropriate boundary conditions set on its flat edges (perfect magnetic conductor (PMC) for the polarization plane and perfect electric conductor (PEC) in the plane perpendicular to it in the case of linear polarization, and PMC for both planes in the case of the radially polarized beam). The linearly polarized wave illumination was implemented in a straightforward way, while the focused radially polarized beam field distribution, obtained in the paraxial approximation [19,20], was numerically corrected. The latter approach allowed implementing highly-focused beams with numerical aperture of 0.4 in air, corresponding to the ~3500 nm beam waist in the studied 300–1000 nm wavelength range, and 1.42 in immersion oil, corresponding to the 550–900 nm waist, which is wavelength-dependent due to tight focusing. The validity of the scattering model was checked benchmarking it against the results for a linearly polarized plane wave on a metallic nanoparticle from the literature [21]. For both illumination scenarios (linear and radial polarizations), the near-field in the vicinity of the particle was numerically evaluated, while the far-field was determined from the near-field using the Stratton-Chu approach [22].

Optical Fourier microscopy

Single particle scattering experiments were performed in reflection using 100 nm gold colloidal nanoparticles. Dispersed nanoparticles were placed in oil between two microscope coverglasses in order to minimize index mismatch. Single nanoparticle spectroscopy was performed using an inverted microscope where the back focal plane of the objective is imaged onto a CCD camera, allowing direct imaging of the scattering pattern of a single nanoparticle. For illumination,

incoherent white light from a tungsten-halogen lamp was filtered spatially with a 5 μm diameter aperture and spectrally with a bandpass filter (532 nm, Chroma), collimated and polarized linearly using a grid polarizer (Throlabs). The polarization can be transformed into radial using a polarization converter (Arcoptix, Switzerland). Linearly or radially polarized light was focused at the particle with a 1.49NA, 100x objective (Nikon). A nanoparticle was collocated with the centre of the beam using a piezostage. For detection, the back-scattered signal was collected by the same objective lens and its back aperture was imaged on a CCD using a 4-lens system. The final images were obtained by subtracting the background signal measured from the coverglass alone from the signal detected with the nanoparticle present. The back-scattering geometry provides a much weaker background, allowing better signal-to-noise ratio than in the forward direction, while allowing the connection to the forward scattering behavior via numerical simulations.

Microwave scanning microscopy

The microwave experiments emulate the optical setup and additionally provide direct measurement of amplitude and phase distributions of the forward scattered waves [23]. The experiments were performed at 9.5 GHz frequency (corresponding to the wavelength $\lambda = 3.2$ cm). A 3.5 mm sphere made from stainless steel was used as a scatterer. Both linearly and radially polarized beams were generated by a widely used conical horn antenna with an aperture diameter of 50 mm attached to a cylindrical waveguide fed by a coaxial cable [24]. The polarization of the beam (either linear or radial) was achieved by exciting different modes of the waveguide. To obtain linear polarization, the antenna is fed by a standard coaxial waveguide connected to the vector network analyzer (VNA, Agilent PNA-L-N5230C), yielding a fundamental H_{11} mode of cylindrical waveguide. The working frequency (9.5 GHz) was chosen

that no other linearly polarized mode can propagate in the waveguide of this size (WC94, inner diameter 24 mm). To obtain radial polarization, the excitation of the first radial mode of the cylindrical waveguide, namely, E_{01}, was used. Again, the waveguide size restricts any other non-polarized cylindrical waveguide modes in the given frequency band. Since Bessel functions of zero order, which describe radial field distribution of H_{11} and E_{01} modes, mimic a Gaussian distribution with at least 97% overlap in amplitude, the field distribution at the antenna aperture imitate linearly or radially polarized Gaussian beam, at least near the centre of the aperture, which are radiated in the free space. The amplitude, phase and polarization profiles of the radiated beams were confirmed by amplitude- and phase-resolved measurements in the near-field zone at a distance of approximately 1.5 wavelength from the antenna aperture. A 3.5 mm sphere made from stainless steel was placed at the distance of one wavelength from the antenna aperture along the beam axis. The measurements of the scattered field were performed in the near-field, recording both phase and amplitude information with a sub-diffraction resolution using a probe mounted on a planar near-field scanner (NSI Inc.) and connected to VNA which allows the signal acquisition in the spectral range up to 100 GHz. Mechanical movement of the probe was controlled by the scanner. A calibrated NSI probe (open end of rectangular waveguide), specifically designed to work in the X-band (8–12 GHz) was used for measuring transverse linearly polarized field. On the other hand, a custom-made coaxial probe was used to measure longitudinal *z*-component of the field. At the first step, the amplitude and phase *x*-*y* maps of the total (incident and scattered) field were measured at the distance $\lambda/2$ from the scatterer. At the second step, the amplitude and phase maps of the incident field (with the scatterer removed) were measured exactly at the same detection plane, again for both polarizations. Using these

data, the amplitude and phase of the scattered field were determined via phase-resolved subtraction.

RESULTS AND DISCUSSION

Conventional optical theorem and complex vectorial beams

The main contribution to the electromagnetic scattering from a subwavelength obstacle usually originates from a dipolar term in the multipolar decomposition. In other words, under linearly polarized plane wave illumination, the particle becomes predominantly polarized along the direction of the incident electrical field (if magnetic response can be neglected) and re-radiates the energy according to a dipolar emission pattern. The highest intensity of the dipolar radiation propagates in the directions, perpendicular to the dipole and, as the result, along the wave vector of the incident linearly polarized wave. Consequently, the forward direction (along the incident wave vector) for scattering is significant. The common formulation of the optical theorem postulates a direct proportionality between the scattering amplitude in the forward direction and the extinction cross-section [1–4]. The situation, however, can be drastically different for vectorial beams which may carry longitudinal field components, optical angular momentum or transverse spin [25]. For example, radially polarized beams have a doughnut-like intensity profile for the transverse polarization directions and, most prominently, a strong longitudinal polarization component along the propagation direction at the beam axis (Fig. 1) [26].

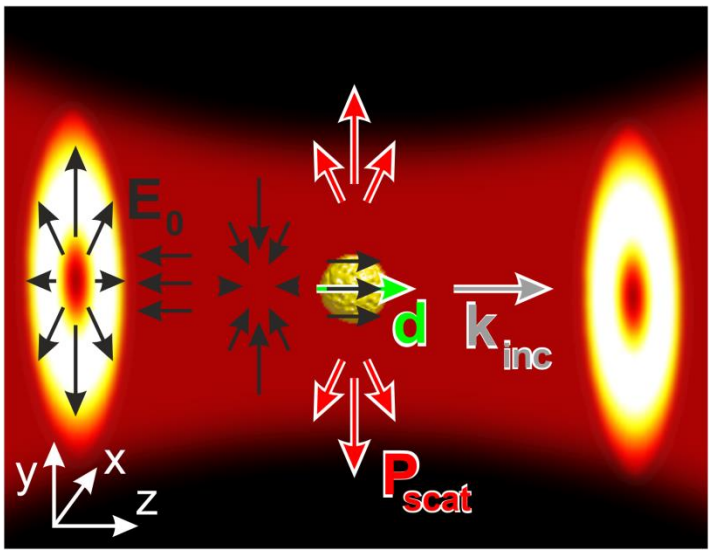

Figure 1 The evolution of the electric field structure of the incident beam, illuminating the nanoparticle from the left (along $\mathbf{k}_{\text{inc}}$), is shown by black arrows together with the dipole moment $\mathbf{d}$ induced in the nanoparticle (green arrow). The intensity of the beam is presented by the color map. The direction of the power flow of the scattered field $\mathbf{P}_{\text{scat}}$ are shown by red-white arrows.

The optical theorem in a textbook formulation provides a straightforward way to calculate the nanoparticle extinction cross-section ($C_{\text{ext}}^{\text{OT}}$), relating its magnitude to the value of the far-field component of the normalized scattered electric field amplitude evaluated in the forward direction (along the incident wave vector) $\mathbf{e}_{\text{scat}}^{\text{far}}\left(\mathbf{k}=\mathbf{k}_{\text{inc}}\right)$ [2–4]:

$$C_{\text{ext}}^{\text{OT}}=\frac{4\pi}{k\varepsilon_{\text{d}}^{1/2}}\,\text{Im}\left\{\mathbf{p}^{*}\cdot\mathbf{e}_{\text{scat}}^{\text{far}}\left(\mathbf{k}=\mathbf{k}_{\text{inc}}\right)\right\}, \tag{1}$$

where $\mathbf{p}$ is the unit vector signifying the polarization of the incident wave, $\mathbf{k}_{\text{inc}}$ and $\mathbf{k}$ are the wavevectors of the incident and scattered waves, respectively, $|\mathbf{k}|=|\mathbf{k}_{\text{inc}}|=2\pi\varepsilon_{\text{d}}^{1/2}/\lambda$, ε_{d} is the

permittivity of the surrounding dielectric, and $\mathbf{e}_{\mathrm{scat}}^{\mathrm{far}}\left(\mathbf{k}=\mathbf{k}_{\mathrm{inc}}\right)$ is related to the scattered electric field $\mathbf{E}_{\mathrm{scat}}^{\mathrm{far}}\left(\mathbf{r}\right)$ as

$$\mathbf{E}_{\mathrm{scat}}^{\mathrm{far}}\left(\mathbf{r}\right)=\left|\mathbf{E}_0\right|\frac{e^{ikr}}{r}\mathbf{e}_{\mathrm{scat}}^{\mathrm{far}}\left(\mathbf{k},\mathbf{k}_{\mathrm{inc}}\right), \tag{2}$$

where $\left|\mathbf{E}_0\right|$ is the amplitude of the incident wave.

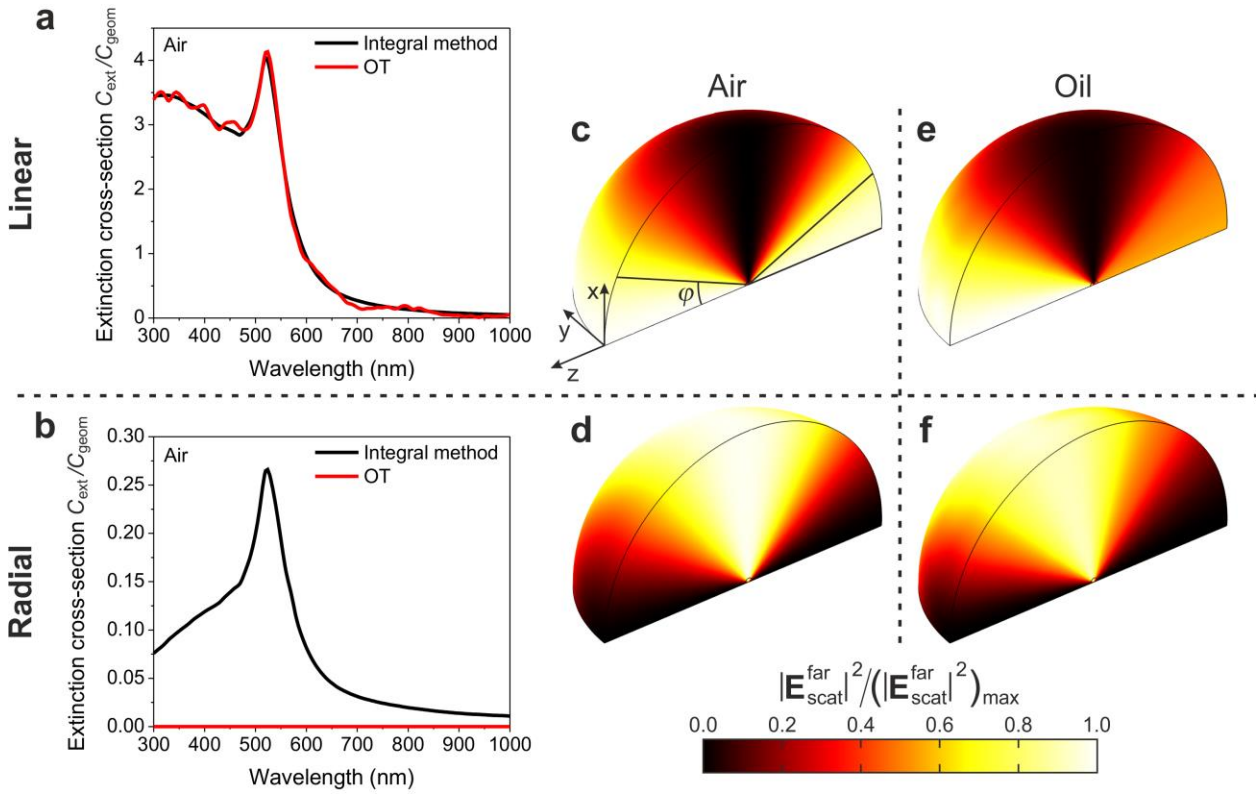

Figure 2 (**a**,**b**) Extinction cross-section spectra of gold nanoparticles with a 50 nm radius (the data are normalized to the geometrical cross-section of the nanoparticle C_{geom}), calculated using the optical theorem (Eq. (1), solid red lines) and generalized with the direct evaluation of the sum of the absorption cross-sections (Eq. (3), black lines) for (**a**) linearly and (**b**) radially polarized illumination beams. (**c**–**f**) Angular scattering spectra of the nanoparticle illuminated by (**c**,**e**) a

plane wave linearly polarized along the *y*-direction and (**d**,**e**) a focused radially polarized beam. The illuminating wave propagates along the *z*-direction and has a wavelength of $\lambda = 530$ nm. The particle is situated in the centre of the diagramme.

Alternatively, the extinction cross-section can be evaluated directly

$$C_{\text{ext}}^{\text{dir}} = C_{\text{abs}}^{\text{dir}} + C_{\text{scat}}^{\text{dir}}, \tag{3}$$

as a sum of the absorption $C_{\text{abs}}^{\text{dir}}$ and scattering $C_{\text{scat}}^{\text{dir}}$ cross-sections. The absorption cross-section can be calculated as an integral of the absorption losses over the nanoparticle volume V, normalized to the incident power flow

$$C_{\text{abs}}^{\text{dir}} = -\frac{\int_V \frac{1}{2}\text{Re}\left\{i\omega\mathbf{E}\cdot\mathbf{D}^*\right\}\text{d}^3\mathbf{r}}{\frac{\varepsilon_{\text{d}}\varepsilon_0 c}{2}\left|\mathbf{E}_0\right|^2} \tag{4}$$

where $\mathbf{E}_0$ and $\mathbf{E}$ are the incident and total electric fields, respectively and $\mathbf{D}$ is the electric displacement. The scattering cross-section can be calculated as an integral of the intensity of the scattered fields over a surface S enclosing the particle, normalized to the same incident field intensity:

$$C_{\text{scat}}^{\text{dir}} = \frac{\oiint_S \mathbf{P}_{\text{scat}}^{\text{far}}\text{d}s}{\frac{\varepsilon_{\text{d}}\varepsilon_0 c}{2}\left|\mathbf{E}_0\right|^2}, \tag{5}$$

where $\mathbf{P}_{\text{scat}}^{\text{far}}$ is the power flow of the scattered waves. We note that other semi-analytical approaches can also be applied for calculations of extinction cross-sections for linearly or radially polarized beams, such as multipole expansion [27]. In the case of the plane wave

illumination of a gold nanoparticle, the direct method of calculation of the extinction cross-section ($C_{\text{ext}}^{\text{dir}}$) and the one based on the optical theorem ($C_{\text{ext}}^{\text{OT}}$) shows excellent agreement (Fig. 2a). The extinction in the spectral range $\lambda = 480 - 550$ nm corresponds to the plasmonic dipolar resonance of the particle. The angular distribution of the far-field scattering has a characteristic shape corresponding to a dipolar radiation pattern, namely, $\cos^2\varphi$, where φ is the scattering angle (Fig. 2c). The scattering dipole is induced along *y*-direction, along the polarization of the incident plane wave, as expected. In the case of the radially polarized incident beam, the situation, however, is drastically different. The wavelength dependence of the extinction cross-section calculated using the direct integration method shows a distinctive peak at the localized surface plasmon resonance of the particle (Fig. 2b, black line), which is in a good agreement with the case of the plane wave excitation (Fig. 2a). At the same time, the extinction cross-section evaluated using the optical theorem given by Eq. (1) is practically zero (Fig. 2b, red line), within a numerical noise defined by the accuracy of the simulations. This means the optical theorem in its common form cannot be applied for such beams. Here we note that for the case of optical beams focused to the dimensions comparable with the size of scattering object, reconsideration of the usual notion of the cross-section is required, as there is a variation of the beam intensity across the object area. For example, in the case of scattering of localized electron wave packets, this has been done through definition of the cross-section through the number of the scattering events, normalizing it to the introduced an effective luminosity of the wave packet [5]. In our case, in an analogy to the above, we used the power extinguished from the beam (equivalent to the number of photons removed from the beam), normalizing it for simplicity to the maximum intensity in the focal plane (Fig. 1).

The apparent contradiction created by the optical theorem described by Eq. (1) can be

understood from the angular scattering diagram (Fig. 2d). For the radially polarized beam, the entire nanoparticle is located in the region of space where the longitudinal component of the incident field dominates (Fig. 1) and the transverse polarization is vanishingly small. Furthermore, it has the the star-like stricture centered at the scatterer position and, therefore, a non-suitable symmetry for an efficient scattering process. Consequently, the dipole moment in the particle is excited only by the longitudinal component along the optical axis, giving rise to a pronounced energy re-radiation directed perpendicular to the beam axis. The dipolar excitation also leads to the related absorption losses in the metal particle. This results in significant non-zero values of scattering and absorption cross-sections, resulting in a considerable value of the extinction cross-section. However, the optical theorem given by Eq. (1) fails to reflect this: due to the symmetry, the re-radiation of the longitudinal dipole in the forward direction (along the dipole axis) is zero and, thus, the optical theorem returns zero extinction cross-section (Fig. 2d). The visual comparison between Figs. 2c and 2d suggests that they are almost perfect replicas of each other, if 90^{o} rotational transformation is applied to one of them. This observation enables drawing intuitive conclusion on the source of the violation of the optical theorem in this formulation. Instead of going along the optical axis, the scattering is deflected by 90^{o}, which is the optimal angle minimizing the forward scattering. Moreover, as can be seen in Figs. 2e and 2f, the violation also takes place in the case of nonresonant excitation at $\lambda = 520$ nm of the nanoparticle in oil (the resonance is moved in this case to $\lambda = 600$ nm) which was further experimentally studied in the next section. In a contrast, in the case of the focused Gaussian beam, along with the longitudinal component (which is the consequence of the focusing, leading to non-zero transverse wavevector components) at the particle position, it will be a substantial, and usually dominating, transverse component. For the former component, as was shown above,

there is a complete violation of the optical theorem, while for the latter component the optical theorem holds, which overall leads to a partial theorem violation. Generally, the stronger the beam is focused, the higher the ratio between the longitudinal and transverse components and the the optical theorem violates more significantly. As was found in Ref. 5 for scattering of vortex electron wave packets, zero forward scattering and yet non-zero overall scattering cross-section can be observed even for scalar localised incident fields of a complex structure with a singularity at the wave packet centre in the transverse plane for axisymmetric scattering. The vectorial nature of the electromagnetic field, however, essentially amplify the effect: the zero divergence of the electromagnetic field at the node of the fields at the beam axis leads to the presence of the longitudinal field components, which result in efficient excitation of the dipole in the nanoparticle along the beam axis and this efficient scattering, resulting in essential extinction simultaneously zero forward scattering.

Experimental investigation of scattering in optical domain using Fourier microscopy

In order to verify the predictions of the numerical modeling, a single particle spectroscopy was performed, allowing direct imaging of the scattering pattern (See Methods). First, linearly polarized excitation was studied with a flat linearly polarized wavefront at the center of the focal spot. These excitation conditions can be directly compared to a plane wave excitation implemented in the simulations. Figures 3b and 3c show an excellent agreement of the experimental and theoretical angular distribution in the back-scattering zone, clearly demonstrating a wave vector distribution having a symmetry with respect to $k_y = 0$ plane with gradually decreasing magnitude towards higher k_y. They directly demonstrate the excitation of a dipole along the excitation polarization direction, as can be seen from the field map cross-sections of the full scattering diagram (Fig. 2e). Due to the nature of the Fourier plane detection,

the number of the wave vectors per $\left(\mathrm{d}k_x, \mathrm{d}k_y\right)$ interval is recorded. Hence, with uniform angular distribution, wave vectors scattered at higher angles have higher density than those close to the optical axis. This explains the higher intensities at the sides of the Fourier images in Figs. 3b and 3c for higher k_x.

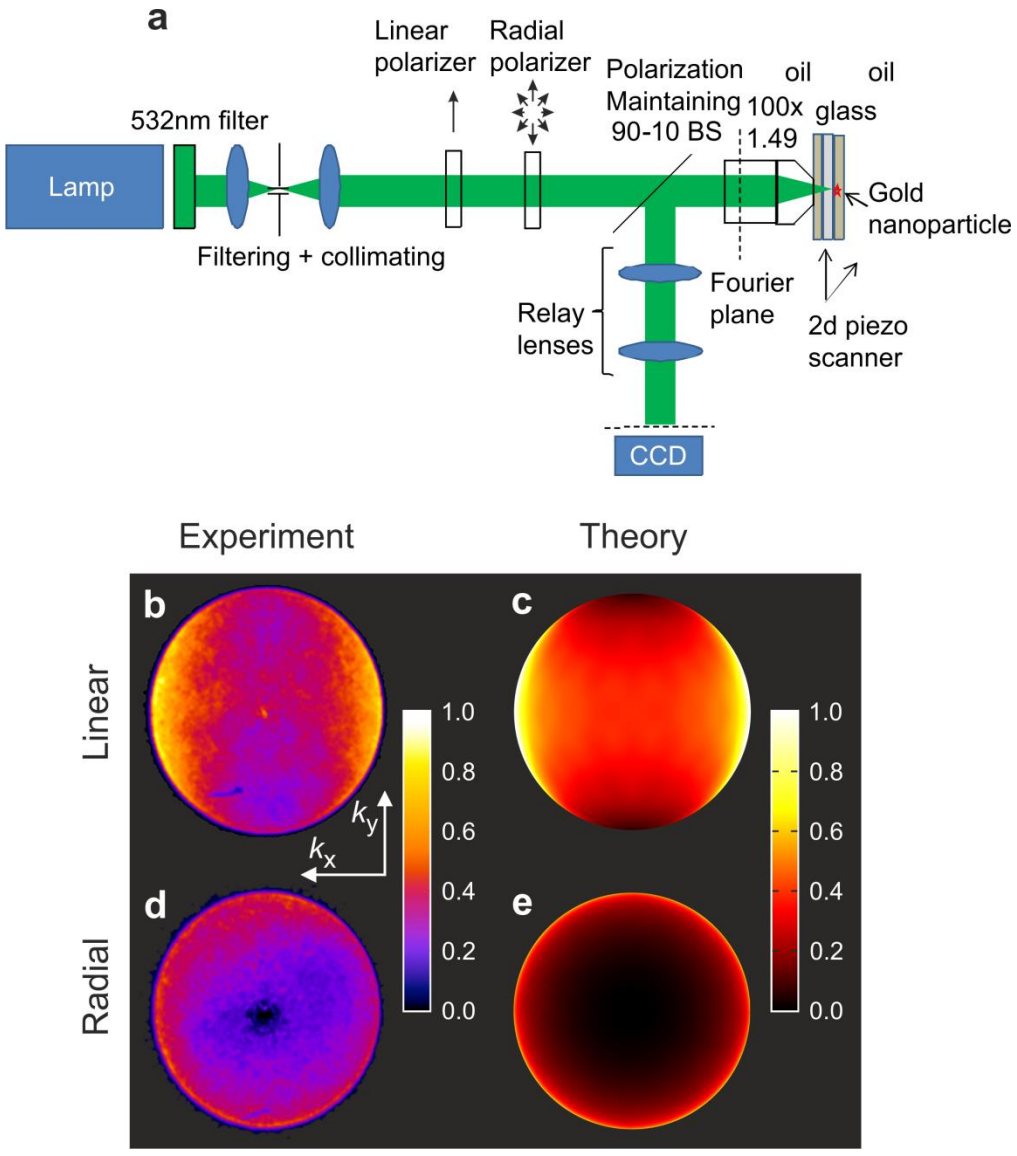

Figure 3 (**a**) Schematic of the Fourier imaging setup used in the experiments. (**b–e**) Angular distribution of the far-field back-scattering in the case of a nanoparticle illuminated by (**b**,**c**) a

linearly polarized plane wave and (**d**,**e**) a radially polarized beam. The results obtained in the optical experiments (**b**,**d**) are compared with the finite element method numerical modeling (**c**,**e**). The parameters of the nanoparticle and illumination are as in Fig. 2.

In the case of the radial polarization, the experimental and numerical observations are again in an excellent agreement (c.f. Figs. 3d and 3e). One can see that the Fourier intensity at the whole central region of the map around $k_x = k_y = 0$ is virtually zero, gradually increasing towards higher k_x and $k_x = k_y$ and clearly possessing a polar angular symmetry. As a subwavelength size of the spherical allows for only the dipolar plasmonic resonance, this provides a clear evidence of the direction of the excited dipole in *z*-axis, which can be easily seen comparing wavevector distributions in the Fourier images with the full scattering diagram in Fig. 2f. Such orientation of the excited dipole inevitably leads to the absolute zero value of the scattering field (and consequently its imaginary part) in the forward direction, along *z*-axis. Hence, we demonstrated a complete violation of the optical theorem in its conventional form for radially polarized beams both experimentally and numerically: while it predicts an extinction cross-section to be zero $C_{\text{ext}}^{\text{OT}} = 0$ (Eq. (1)) on the basis of the zero scattering along the incident wave vector, considerable extinction cross-section of the particle is observed with strong scattering of the incident radially polarized beam in the direction of large k_x and k_y wave vectors.

Scanning microscopy of scattered field in microwave domain

The microwave experiments on scattering emulate the optical setup and provide a direct measurement of amplitude and phase distributions of the scattered waves [23]. The distributions

of the scattered field amplitude in the forward direction demonstrate an extremely good agreement with modeling (cf. Fig. 4b, 4c and 4d, 4e). For the linearly polarized illumination, the radiation profile corresponds to the dipolar moment excited along the direction of the incident polarization (Fig. 4b). On the other hand, the radiation profile in the case of the radially polarized illumination provides an unambiguous evidence of the dipole moment excitation in *z*-direction, along the beam axis (Fig. 4c). Again, the conventional formulation of the optical theorem is violated in these conditions: an essential scattering signal (and, therefore, considerable extinction cross-section) is evident, while Eq. (1) predicts zero extinction on the basis of zero field measured in the forward direction (along *z*-axis).

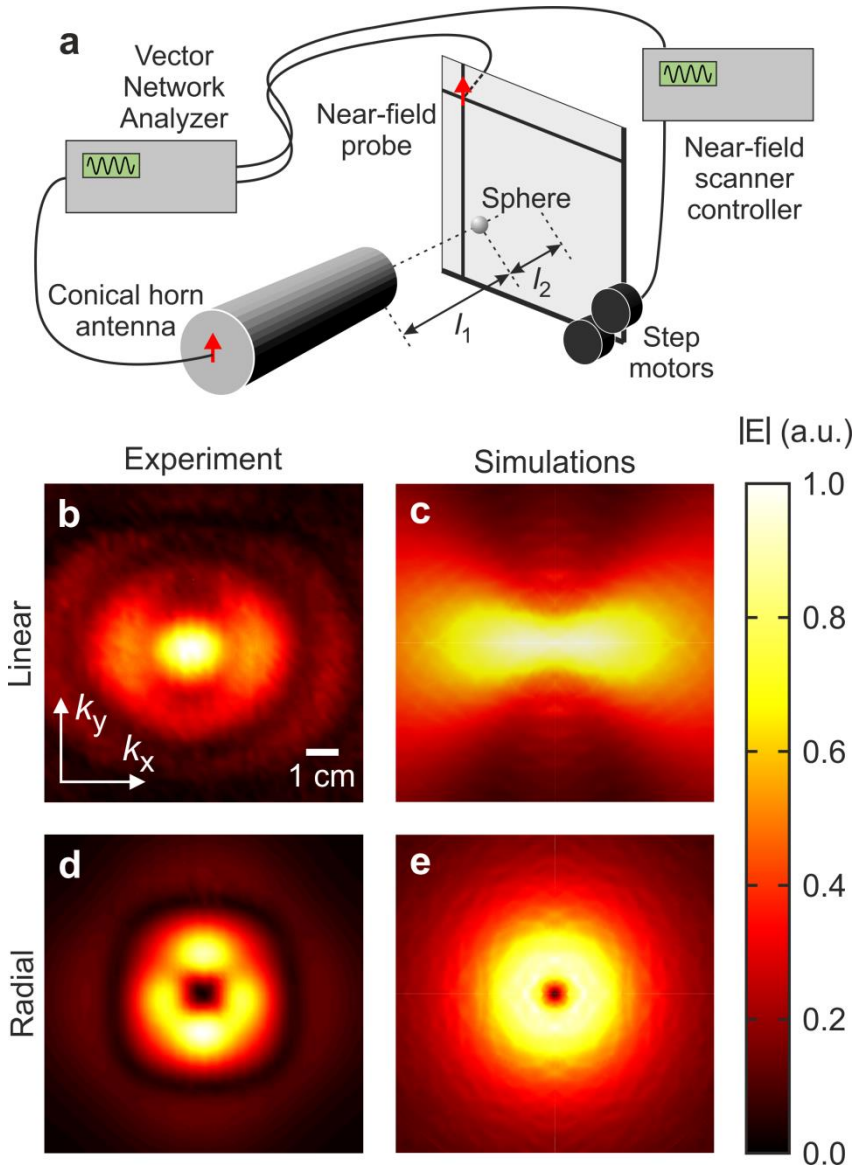

Figure 4 (**a**) Near-field scanning setup used in the microwave experiments. (**b–e**) Near-field distribution of forward scattering on a 3.5 mm metallic nanoparticle recalculated from the amplitude and phase maps measured at a distance of $l_2 = 14.5$ mm from the particle centre in the case of (**a**,**b**) a linearly polarized plane wave and (**c**,**d**) a radially polarized beam. Microwave radiation frequency is 9.5 GHz, corresponding to $\lambda = 3.2$ mm ($l_1 \approx \lambda$). The results obtained in the microwave experiments (**b**,**d**) are compared with the finite element method numerical modeling (**c**,**e**).

The fact that the facet of the of the probe rectangular waveguide lie in the measurement plane and, therefore, has a lower acceptance of the incident wave at higher angles leads to the smaller measured signal in this region, which explains the related difference in the experimental and theoretical field maps (cf. Figs. 4b,d and Figs. 4c,e). The metallic sphere was held in the setup by a sample holder made of a plastic foam sheet. The sheet is nearly transparent for microwaves ($\varepsilon \sim 1.1$) and, thus, did not essentially influence the results, although its presence can explain minor radial interference fringes observed in the experimental field maps (Figs. 4b,d).

Generalization of the optical theorem

These numerical and experimental observations strongly call for the necessity of the development and application of generalized formulations of the optical theorem [28]. This can be achieved considering a relation linking extinction to incident ($\mathbf{E}_0(\mathbf{r})$, $\mathbf{H}_0(\mathbf{r})$) and total ($\mathbf{E}(\mathbf{r})$, $\mathbf{H}(\mathbf{r})$) fields valid for any vectorial structure of the field [28]

$$C_{\text{ext}}^{\text{GOT}} = \frac{1}{\varepsilon_{\text{d}} |\mathbf{E}_0|^2} \operatorname{Im}\left\{ \int_V d^3\mathbf{r} k(\mathbf{r}) \left[\mathbf{E}_0^*(\mathbf{r}) \cdot \mathbf{E}(\mathbf{r}) \eta(\mathbf{r}) + \mathbf{H}_0^*(\mathbf{r}) \cdot \mathbf{H}(\mathbf{r}) \chi(\mathbf{r}) \right] \right\}, \tag{6}$$

where $\eta(\mathbf{r})$ and $\chi(\mathbf{r})$ are the electric and magnetic susceptibilities of the scatterer and the integration is taken over the scatterer volume V. The incident beam in free space is then represented by an arbitrary-complex vectorial structure allowed by the Maxwell's equations and treated as a superposition of plane waves (generally allowing also evanescent components) with amplitudes $\mathbf{e}(\mathbf{k})$. The extinction cross-section can then be expressed by projecting the amplitudes of scattered components $\mathbf{e}(\mathbf{k}_1)\mathbf{A}(\mathbf{k}_1, \mathbf{k}_2^*)$ from each of the partial incident waves

$\mathbf{e}(\mathbf{k}_1)$ on all other incident components $\mathbf{e}(\mathbf{k}_2)$ and integrating over all possible directional combinations of $\mathbf{k}_1$ and $\mathbf{k}_2$:

$$C_{\text{ext}}^{\text{GOT}} = \frac{\omega}{\varepsilon_{\text{d}} c |\mathbf{E}_0|^2} \text{Im}\left\{ \int \text{d}^2 k_{1\|} \int \text{d}^2 k_{2\|} e_\beta^*(\mathbf{k}_2) e_\alpha(\mathbf{k}_1) A_{\alpha\beta}(\mathbf{k}_1, \mathbf{k}_2^*) \right\}. \quad (7)$$

Here, $A_{\alpha\beta}(\mathbf{k}_1, \mathbf{k}_2^*)$ are the components of the scattering amplitude tensor $\mathbf{A}(\mathbf{k}_1, \mathbf{k}_2^*)$, double indexes imply summation and || denotes the projection on the *z*-axis. Applying this approach to the scattering of both linearly and radially polarized illumination, it was found that the generalized optical theorem (Eqs. (6) and (7)) is in excellent agreement with the direct evaluation of the extinction cross-section using Eqs. (3–5) (Figs. 5a,b), revealing its validity even for the vectorial case. We note that in the derivation of the generalized optical theorem no assumptions on the shape of the incident beam and the scattering object were made, e.g., complex fields including evanescent components and the objects with an optical response dominated by magnetic dipoles or electric quadrupoles can be considered. The form of the optical theorem given by Eq. (6) is very convenient for approaching the problem with numerical simulations, allowing straightforward integrations of the resulting electromagnetic fields. On the other side, the form given by Eq. (7) is more suitable for analytical and semi-analytical calculations. Finding $\mathbf{A}(\mathbf{k}_1, \mathbf{k}_2^*)$ and evaluation of scattering of a plane wave by an object of a given shape are generally within the capabilities of analytical calculations (see e.g. [29]). Then, the double integration over the wave vectors for simple scatterers can be done analytically, otherwise numerical evaluation can be performed using standard software.

The optical theorem was further tested in the case of scattering of focused azimuthally polarized beam (with the same parameters as for radially polarized beam in Fig. (2)) on a 100 nm

spherical gold nanoparticle. Numerical modeling shown that the generalized version of the optical theorem (Eqs. (6) and (7), dashed green line in Fig. 5c) gives the correct prediction of the value of the extinction cross-section, while its conventional formulation (Eq. (1), solid red line in Fig. 5c) proves to be inadequate. Due to the vectorial structure of the beam signified by the absence the electric terms in its multipole decomposition [30], the electric resonances which play a leading role in the optical response of a spherical plasmonic particle are not excited. This leads to much lower extinction cross-section values in comparison to linearly and radially polarized excitation (cf. Fig. 5c and Figs. 5a,b). Particularly, the peak at a wavelength of 520 nm, corresponding to the dipole resonance is no longer present for azimuthal polarization. The observed small increase in the extinction cross-section towards the shorter wavelengths is related to the increase of the absorption in metal.

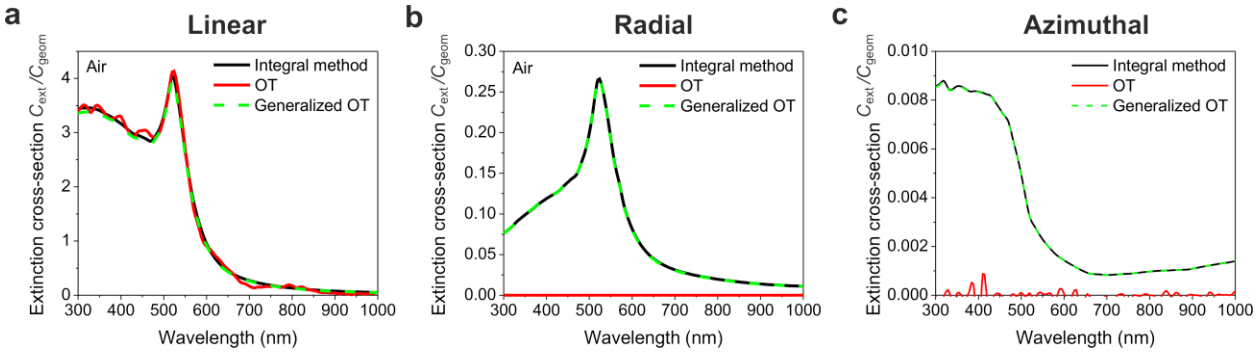

Figure 5 Extinction cross-section spectra of gold nanoparticles with a 50 nm radius, calculated using the optical theorem (OT) Eq. (1) (solid red line), generalized OT Eqs. (6,7) (dashed green line) and direct evaluation of the sum of the absorption Eq. (4) and scattering Eq. (5) cross-sections (black line).

CONCLUSIONS

A violation of the standard formulation of the optical theorem was demonstrated both experimentally and numerically for the illumination with radially polarized electromagnetic

beams featuring strong longitudinal field components. Optical measurements were complemented by experiments in the microwave domain. The experiments, together with comprehensive numerical modeling, show a clear evidence of the breakdown of the textbook version of the optical theorem. The origin of the breakdown has been identified to be the presence of longitudinal field components in the complex vector-beams. Rather than creating a paradox, this violation provides the evidence of the need for reconsideration of required conditions for satisfying the theorem which is originally formulated for scalar and transverse vectorial waves. The generalized formulations of the optical theorem [28] was shown to be in agreement with our numerical and experimental results. Longitudinal field components and related transverse optical spin of surface and guided modes leads to impossible for transverse waves inverse photonic spin-Hall effect [31] and emergence of lateral optical forces [32].Finally, we would like to point out that a similar violation should happen for another important type of complex beams – vortex beams (having a non-zero orbital angular momentum). In an analogy to radially- and azimuthally-polarized beams, vortex beams have zero transverse electric field components. Due to the symmetry of the problem, the forward scattering for vortex beams is zero, and so is the extinction cross-section given by the standard expression for the optical theorem, while in fact the extinction cross-section is non-zero at least due the high-order (e.g., quadrupolar) scattering effects, and, if present, due to absorption.

In order to underline the importance of generalisation of well established physical rules on the novel phenomena, for which the original form of the rule is no longer applicable it is interesting to draw the attention to a phenomena having very close parallels to the one studied in the manuscript, yet from a completely different area of physics. Particularly, this is the generalisation of the Born approximation for the scattering of electrons on energy potentials in

the case of localized electron wave packets instead of plane waves [33,5]. Apart from the reconsidering the definition of a cross-section when the incident field localisation is comparable with the scatterer size, as discussed above, it was found that for twisted (vortex) incident electron wave packets, if the impact parameter of the incident wave packet is zero (the beam axis goes through the center of the scattering potential), the forward scattering is zero as well while the overall cross-section is not, which is in complete analogy with the violation of the optical theorem for the radial and azimuthal optical beams considered here.

As the optical theorem in different forms is frequently used in a broad range of applications, such as imaging, nanoparticle manipulation, communications, and radar detection, as well as in other physics domains, e.g., for quantum scattering [34], these findings demonstrate that careful reconsideration of required conditions and introduction of additional degrees of freedom is of key importance. Understanding and generalization of the optical theorem applicability can broaden the span of its applications. For example, consideration of spin-flip in electron scattering process could introduce another (vectorial) degree of freedom, which could have remarkable implications to relations between the total extinction and forward scattering.

ACKNOWLEDGMENTS

This work was supported in part by EPSRC (UK) and ERC (project 789340). P.G. acknowledges the support by a TAU Rector Grant and the German-Israeli Foundation (GIF, grant number 2399). A.Z. acknowledges support from the Royal Society and the Wolfson Foundation. A.K. and R.D. thank Mr. Alexander E. Ageyskiy for help with the microwave experiments.

REFERENCES

1. M. Born and E. Wolf, *Principles of Optics*, 7th (Expanded) Edition, (Cambridge University Press, New York, 2002).

2. J. D. Jackson, *Classical Electrodynamics*, 3rd Edition, (Wiley, 1999).

3. C. F. Bohren and D. R. Huffman, *Absorption and Scvattering of Light by Small Particles*, (Wiley, 1998).

4. M. I. Mishchenko, L. D. Travis, and A. A. Lacis, *Scattering, Absorption, and Emission of Light by Small Particles*, (Cambridge University Press, Cambridge, 2002).

5. D. V. Karlovets, G. L. Kotkin, V. G. Serbo, and A. Surzhykov, "Scattering of twisted electron wave packets by atoms in the Born approximation," Phys. Rev. A **95**, 032703 (2017).

6. R. G. Newton, "Optical theorem and beyond," Am. J. Phys. **44**, 639–642 (1976).

7. J. A. Lock, J. T. Hodges, and G. Gouesbet, "Failure of the optical theorem for Gaussian-beam scattering by a spherical particle," J. Opt. Soc. Am. A **12**, 2708–2715 (1995).

8. K. Sendur and A. Sahinöz, "Interaction of radially polarized focused light with a prolate spheroidal nanoparticle," Opt. Express **17**, 10910–10925 (2009).

9. A. Normatov, P. Ginzburg, N. Berkovitch, G. M. Lerman, A. Yanai, U. Levy, and M. Orenstein, "Efficient coupling and field enhancement for the nano-scale: plasmonic needle", Opt. Express **18**, 14079–14086 (2010).

10. G. M. Lerman, A. Yanai, and U. Levy, "Demonstration of nanofocusing by the use of plasmonic lens illuminated with radially polarized light," Nano Lett. **9**(5), 2139–2143 (2009).

11. W. Chen, D. C. Abeysinghe, R. L. Nelson, and Q. Zhan, "Plasmonic lens made of multiple concentric metallic rings under radially polarized illumination," Nano Lett. **9**(12), 4320–4325 (2009).

12. E. A. Marengo and J. Tu, "Optical theorem for transmission lines," Prog. Electromagn. Res. B **61**, 253–268 (2014).

13. E. A. Marengo and J. Tu, "Generalized optical theorem in the time domain," Prog. Electromagn. Res. B **65**, 1–18 (2016).

14. E. A. Marengo, “A new theory of the generalized optical theorem in anisotropic media,” IEEE Trans. Antennas Propagat. **61**, 2164–2179 (2013).

15. D. K. Dacol and D. G. Roy, “Generalized optical theorem for scattering in inhomogeneous media,” Phys. Rev. E **72**, 036609 (2005).

16. D. Halliday and A. Curtis, “Generalized optical theorem for surface waves and layered media,” Phys. Rev. E **79**, 056603 (2008).

17. P. S. Carney, “The optical theorem with fields containing evanescent waves,” J. Mod. Opt. **46**, 891–899 (1999).

18. P. B. Johnson and R. W. Christy, "Optical constants of noble metals," Phys. Rev. B **6**, 99–107 (1939).

19. N. M. Mojarad and M. Agio, "Tailoring the excitation of localized surface plasmon-polariton resonances by focusing radially polarized beams," Opt. Express **17**, 117–122 (2009).

20. G. Gouesbet, J. A.Lock, and G. Grehan, “Generalized Lorenz–Mie theories and description of electromagnetic arbitrary shaped beams: Localized approximations and localized beam models, a review”, J. Quant. Spectrosc. Radiat. Transfer **112**, 1–27 (2011).

21. J. Parsons, C. P. Burrows, J. R. Sambles, and W. L. Barnes, “A comparison of techniques used to simulate the scattering of electromagnetic radiation by metallic nanostructures”, J. Mod. Opt. **57** (5), 356–365 (2010).

22. J. A. Stratton and L. J. Chu, "Diffrection theory of electromagnetic waves," Phys. Rev. **36**, 4370–4379 (1972).

23. P. V. Kapitanova, P. Ginzburg, F. J. Rodriguez-Fortuno, D. S. Filonov, P. M. Voroshilov, P. A. Belov, A. N. Poddubny, Y. S. Kivshar, G. A. Wurtz, and A. V. Zayats, “Photonic spin Hall effect in hyperbolic metamaterials for polarization-controlled routing of subwavelength modes”, Nat. Commun. **5**, 3226 (2014).

24. C. A. Balanis, *Antenna Theory: Analysis and Design*, Wiley-Interscience; 3 edition , 2005.

25. K. Y. Bliokh, F. J. Rodríguez-Fortuño, F. Nori, and A. V. Zayats, “Spin–orbit interactions of light,” Nat. Phot. **9**(12), 796–808 (2015).

26. R. Martínez-Herrero, P.M. Mejías, I. Juvells, and A. Carnicer, “Transverse and longitudinal components of the propagating and evanescent waves associated to radially polarized nonparaxial fields”, Appl. Phys. B **106**, 151–159 (2012).

27. N. M. Mojarad and M. Agio, “Tailoring the excitation of localized surface plasmon-polariton resonances by focusing radially-polarized beams,” Opt. Express **17**, 117–122 (2008).

28. D. R. Lytle II, P. S. Carney, J. C. Schotland, and E. Wolf, "Generalized optical theorem for reflection, transmission, and extinction of power for electromagnetic fields," Phys. Rev. E **71**, 056610 (2005).

29. K. N. Liou, Q. Cai, J. B. Pollack, and J. N. Cuzzi, “Light scattering by randomly oriented cubes and parallelepipeds,” Appl. Opt. **22**, 3001 (1983).

30. S. Orlov, U. Peschel, T. Bauer, and P. Banzer, “Analytical expansion of highly focused vector beams into vector spherical harmonics and its application to Mie scattering,” Phys. Rev. A **85**, 063825 (2012).

31. D. O’Connor, P. Ginzburg, F. J. Rodríguez-Fortuño, G. A. Wurtz, and A. V. Zayats, “Spin–orbit coupling in surface plasmon scattering by nanostructures,” Nat. Commun. **5**, 5327 (2014).

32. F. J. Rodríguez-Fortuño, N. Engheta, A. Martínez, and A. V. Zayats, “Lateral forces on circularly polarizable particles near a surface,” Nat. Commun. **6**, 8799 (2015).

33. D. V. Karlovets, G. L. Kotkin, and V. G. Serbo, “Scattering of wave packets on atoms in the Born approximation,” Phys. Rev. A **92**, 052703 (2015).

34. J. R Taylor, *Scattering Theory: The Quantum Theory of Nonrelativistic Collisions*, Dover Publications Inc., 2006.